Analysis of fine structure in the nuclear continuum

A. Shevchenko,[1] J. Carter,[2] G. R. J. Cooper,[3] R. W. Fearick,[4] Y. Kalmykov,[1] P. von Neumann-Cosel,[1,*] V. Yu. Ponomarev,[1,†] A. Richter,[1] I. Usman,[2] and J. Wambach[1]

[1]*Institut für Kernphysik, Technische Universität Darmstadt, D-64289, Darmstadt, Germany*
[2]*School of Physics, University of the Witwatersrand, P. O. Wits, Johannesburg 2050, South Africa*
[3]*School of Earth Sciences, University of the Witwatersrand, P. O. Wits, Johannesburg 2050, South Africa*
[4]*Department of Physics, University of Cape Town, Rondebosch 7700, South Africa*

Fine structure has been shown to be a general phenomenon of nuclear giant resonances of different multipolarities over a wide mass range. In this article we assess various techniques that have been proposed to extract quantitative information from the fine structure in terms of characteristic scales. These include the so-called local scaling dimension, the entropy index method, Fourier analysis, and continuous and discrete wavelet transforms. As an example, results on the isoscalar giant quadrupole resonance in ^{208}Pb from high-energy-resolution inelastic proton scattering and calculations with the quasiparticle-phonon model are analyzed. Wavelet analysis, both continuous and discrete, of the spectra is shown to be a powerful tool to extract the magnitude and localization of characteristic scales.

I. INTRODUCTION

Electric and magnetic nuclear giant resonances are well-known examples of the striking behavior of an interacting system of fermions to form collective modes [1]. Over the years, much experimental work has gone into establishing an understanding of the global behavior of the gross features, such as centroid energies and widths, of these resonances. It is generally accepted that the width Γ of the resonances mainly results from two mechanisms: direct particle emission from one-particle one-hole (1p-1h) configurations giving rise to an escape width $\Gamma^\uparrow$ and the evolution of these 1p-1h configurations into more complicated two-particle two-hole (2p-2h) and finally to np-nh configurations giving rise to a spreading width $\Gamma^\downarrow$. This latter scheme has implicit in it a hierarchy of widths and time scales resulting in a fragmentation of the giant resonance strength in a hierarchical manner [2]. An important theoretical problem is to explain the nature of couplings between the levels in this hierarchy and to predict the scales of the fragmentation of the strength which thus arise from it.

Already about 30 years ago it became apparent from high-energy-resolution inelastic electron-scattering experiments [3,4] that there was considerable fine structure superimposed on the broad bump of the isoscalar giant quadrupole resonance (ISGQR) in ^{208}Pb. Further studies [5] have shown that such fine structure is physical in nature and also appears in other reaction channels. Recent high-energy-resolution (p, p') measurements demonstrated the fine structure in a wide range of nuclei for the ISGQR [6]. It has also been observed in other types of resonances like the isovector giant dipole resonance [7,8], the magnetic quadrupole resonance [9], or the spin-isospinflip Gamow-Teller mode [10], establishing it as a generic phenomenon of nuclei.

Nevertheless, a serious experimental problem has been the quantitative extraction of the scales of this fragmentation. A lower limit on observable scales is placed by the experimental resolution. The recent experiments have been made possible by the exploitation of high-energy-resolution magnetic spectrometers and particle beams with energies of several hundred MeV allowing for energy resolutions of a few tens of keV. The problem then is to determine scales that occur in the range between the experimental resolution and the broad envelope of the resonances (typically several MeV).

Early on, an attempt was made to analyze the data on the fine structure of the ISGQR in ^{208}Pb observed in Refs. [3,4] in terms of a doorway-state model [11]. It could be shown that in this case the spreading width dominates over the escape width but the deduced scales depended strongly on the assumptions about the (unknown) number of doorway states. In this work, we concentrate on the evaluation of several new methods proposed for the extraction of such scales, *viz.* the local scaling dimension approach [12], the entropy index method [13], and the use of wavelet techniques [6], and compare the latter to older techniques such as Fourier analysis. As a test case, we investigate data on the ISGQR in ^{208}Pb from high-energy-resolution (p, p') experiments and a calculation of the corresponding isoscalar $E2$ strength function within the quasiparticle-phonon model (QPM). Although a more extensive data set and still other calculations are available, we restrict ourselves to these examples because the focus of the article is to evaluate the advantages and limitations of the different techniques for an extraction of characteristic scales. Possible conclusions on the nature of these scales and their implications for the decay of giant resonances are subject of a subsequent article.

The article is organized as follows: in Sec. II we briefly present the data sets used during the analysis. As pointed out above, these are an experimental spectrum and a theoretical

---

*vnc@ikp.tu-darmstadt.de
†Permanent address: Bogoliubov Laboratory for Theoretical Physics, JINR, Dubna, Russia.

strength function. Both can be analyzed with the same techniques so that the scales determined can be compared on the same basis, without first establishing a translation mechanism between the language of experiment and theory. We also discuss the relations of scale values deduced from the different methods and what is meant by scale in this regard. In the following Secs. III to VI the above-mentioned techniques are applied to the data and their results are discussed. Finally, Sec. VII contains some concluding remarks.

II. DATA AND ANALYSIS

A. Data sets

In this article, we focus on the data analysis techniques used to extract characteristic energy scales of fine structure in the region of the ISGQR. For this purpose we restrict our interest to two sets of data: an experimental spectrum measured in inelastic proton scattering and a theoretical calculation of the isoscalar giant quadrupole strength, calculated within the framework of the QPM [14].

Experimental data were obtained by high-energy-resolution (p, p') measurements performed [6] using the K600 magnetic spectrometer of the cyclotron of iThemba LABS, Somerset West, South Africa. Data were taken at an incident proton energy of 200 MeV using an isotopically enriched ($>95\%$) ^{208}Pb target of thickness 0.75 mg/cm^2. An energy resolution of about 45 keV (full width at half maximum, FWHM) was achieved. A measurement of the scattered particle energy spectrum is shown in the top part of Fig. 1 corresponding to a scattering angle of 8°, chosen at the first maximum of the $\Delta L = 2$ angular distribution. An extended view of the excitation energy region $E_x = 8$–13 MeV shows pronounced fine structure in the region of the ISGQR, which peaks at about 10.5 MeV in ^{208}Pb.

Also shown in Fig. 1 is the theoretical prediction of the ISGQR strength distribution calculated within the QPM. Details on the calculation can be found in Ref. [6]. This spectrum has been convoluted with a Gaussian of width 50 keV (FWHM) that is representative of the experimental energy resolution.

The purpose of the analysis techniques to be discussed is to extract from the data some information on the energy scales that characterize the fluctuations in the cross section that constitute the fine structure of the ISGQR in ^{208}Pb. These energy scales can then be compared to scales similarly extracted from theoretical calculations of the ISGQR strength. Our basic approach is to apply a similar analysis technique to both experimental and theoretical "data" and make a comparison using scales obtained on an equal footing, thus circumventing some of the difficulties in the interpretation of these scales.

B. Lengthlike and widthlike scales

There are two basic meanings of "scale" in the literature that, confusingly, are often used almost interchangeably. On the one hand, well-established methods of analysis, such as
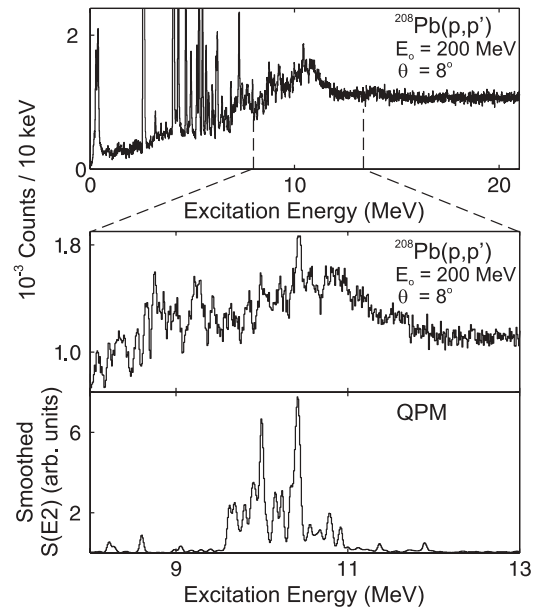

FIG. 1. Data used in the analysis. (Top panel) Experimental energy spectrum of 200 MeV protons scattered from ^{208}Pb at $\Theta = 8°$. The region of interest, where the ISGQR is concentrated, is expanded in the middle panel. (Bottom panel) Theoretical strength function calculated within the framework of the QPM. The latter has been convoluted with a Gaussian of 50-keV FWHM, which is representative of the experimental energy resolution.

autocorrelation analysis, are used to extract lengthlike scales from spectra, i.e., "distances" between features, which in a model-dependent analysis yields information on, for example, level densities [15]. On the other hand, widthlike scales are also discussed, as in the hierarchy of decay widths in the damping of giant resonances. For given features of a spectrum these two types of scales will have different values. At the same time they are related to one another, and both can occur together in the same data set. By comparing only the scales found with a specific technique for different data sets this interpretative problem can be avoided. We thus do not rely on some internal idea of scale for a particular data set, for instance scales that might be built into some theoretical model.

Another problem arises in relating the energy scales determined using one technique to those of another. This can only really be approached empirically by comparing results obtained with the different techniques for some model data set. A related problem occurs in the wavelet analysis described below, where different wavelet families have different intrinsic scales. To avoid this ambiguity in scale, we have used a common scale for all wavelet families. Thus, rather than the intrinsic wavelet scale s_{int}, we use the value $s = \lambda_w s_{int}$ where the constant λ_w depends on the particular wavelet family. This factor λ_w is determined, as detailed, e.g., by Torrence and Compo [16], by the analysis of the wavelet decomposition of a sinusoid of known period. With this procedure all wavelet families give the same scales in the analysis of a sinusoid. Because of the physics nature of the scales in the present problem we prefer to extract widthlike scales derived empirically from wavelet transforms of Lorentzian peaks. This

scale, called the "wavelet scale" corresponds to the FWHM of the peak.

A final problem occurs in Fourier transform pairs. Because we report scales s in terms of energy rather than 1/energy we have a choice to regard $1/s$ or $2\pi/s$ as conjugate to the energy E. In the spirit of regarding the scale as a "length-like" quantity we have chosen the latter ($2\pi/s$), which we call a "Fourier scale."

III. LOCAL SCALING DIMENSION (LSD)

A. Method

Aiba and Matsuo [12] have proposed a technique for the analysis of fine structure by the determination of a local scaling dimension calculated from a subpartitioning of the data. This scheme is based on the scaling analysis of a series having a self-similar multifractal character.

Given a strength function $S(E)$ defined over some energy range $\Delta E = [E_{\min}, E_{\max}]$, the data are partitioned on a number of different scales. At each scale δE the data are rebinned into a number $N = \Delta E/\delta E$ bins. The strength of the nth bin is denoted $p_n = \sum_{i \in n} S_i$. From the set of binned data $\{p_i\}$ a partition function of order m is determined by

$$\chi_m(\delta E) = \sum_{i=1}^{N} p_i^m = N \langle p_i^m \rangle, \tag{1}$$

where $\langle \ldots \rangle$ denotes an average.

With this formulation, a statistical distribution of fluctuations in the data results in all p_i being approximately the same, $p_i \propto 1/N \propto \delta E$ and hence $\chi_m(\delta E) \propto (\delta E)^{m-1}$. In the other extreme, if all strength S is located at one energy, then $\chi_m(\delta E) = S$ for all δE. For a fractal distribution of fluctuations, the partition function will have a nontrivial scaling depending on some fractal dimension. When dealing with more general data having specific energy scales, the fractal dimension is extended by the definition of a local scaling dimension $D_m(\delta E)$ to characterize the type of fluctuations that might arise in the damping of giant resonances [12],

$$D_m(\delta E) = \frac{1}{m-1} \frac{\partial \ln \chi_m(\delta E)}{\partial \ln \delta E}. \tag{2}$$

A change in local scaling dimension as a function of energy scale then reveals a characteristic scale of the data. The method has been used to extract characteristic scales from shell-model calculations of the ISGQR and the isovector giant quadrupole resonance (IVGQR) in ^{40}Ca [17].

Careful treatment of the boundaries of the data are needed [12] to avoid artifacts in the results. In our case, the method was applied to multiple repeats of the region of interest, thus giving, essentially, periodic boundary conditions. The results are nevertheless very sensitive to small shifts in the boundary.

B. Results

Application of this method to the data is shown in Fig. 2. Calculations are shown for values $m = 2$ or 3 of the order of the partition function as examples. Differences are small.
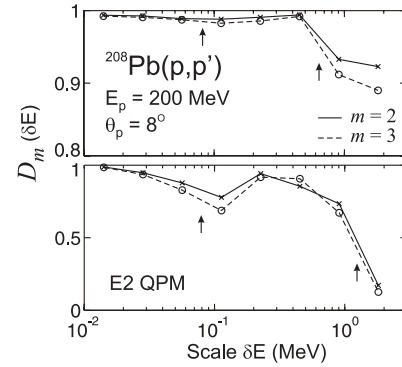

FIG. 2. Analysis by the local scaling dimension method, Eq. (2). The top and bottom panels show the results the experimental and theoretical spectrum, respectively. Open circles and crosses correspond to values $m = 2$ and 3 of the order of the partition function, respectively. The solid and dashed lines are to guide the eye only. Arrows indicate possible scales at 80 keV, 600 keV (top), and 80 keV, 1.3 MeV (bottom) revealed by the analysis.

It is not very obvious on how to interpret these plots in terms of scales. Taking variations of D_m as a criterion, scales in the experimental spectrum are indicated at about 80 and 600 keV and in the theoretical spectrum at about 80 and 1.3 MeV, marked by arrows in Fig. 2. However, it is clear from the plots in Fig. 2 that these scales are not well discriminated and the ability of the method to resolve scales is limited. Furthermore, numerical studies suggest that the method is not stable with respect to different forms of background in experimental spectra.

IV. THE ENTROPY INDEX METHOD (EIM)

A. Method

Another technique [13] proposed for the multiscale analysis of the fine structure problem and based on a subpartitioning of the data is the entropy index method (EIM). This method defines an entropy derived from a measure of fluctuations of a spectrum. This measure is determined on a range of scales, and changes in the entropy with scale signal the appearance of characteristic scales in the data. An advantage of this method is its model independence—no assumption is made *a priori* about the number of scales in the data or their values.

The data set $\sigma(E)$ is rebinned for each scale as described in Sec. III A. For each bin j a coefficient at scale δE is defined as

$$D_j(\delta E) = \int_{E_{j-1}}^{E_j} \sigma(E) \Psi_j(E) \, dE, \tag{3}$$

where $E_j = E_{\min} + j\delta E$. Here, $\Psi_j(E)$ is a windowing function that is nonzero only within the interval j and has a vanishing zeroth moment, i.e., $\int \Psi(E) dE = 0$. An antisymmetric function is chosen, the simplest being the step function

$$\Psi_j(E) = \mathrm{sign}\left[E - \left(j - \frac{1}{2} \right) \delta E \right], \tag{4}$$
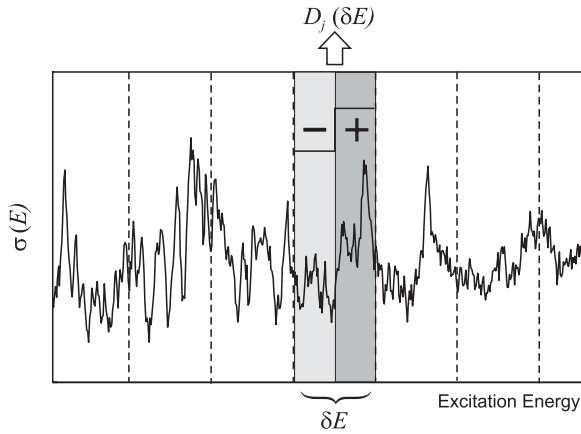
FIG. 3. Illustration of the extraction of a coefficient at scale δE in the entropy index method. The coefficient $D_j(\delta E)$, Eq. (3), is determined by folding the spectrum $\sigma(E)$ with the step function, Eq. (4), and corresponds to the difference between the sums over the dark- and light-gray shaded region in the spectrum.

which changes sign midway across the interval. The process of applying such a windowing function to the data is illustrated in Fig. 3.

The coefficients $D_j(\delta E)$ thus found form a coarse-grained derivative of the data $\sigma(E)$. If the fluctuations in the data are of the order of scale δE then the coefficients will be significant; if the fluctuations are of much larger or smaller scale then the coefficients will be small. This assessment is made by defining a scale-dependent entropy from the data. First the coefficients are normalized by the averages of their absolute values,

$$W_j(\delta E) = \frac{|D_j|}{\langle |D_j| \rangle}, \qquad (5)$$

where

$$\langle |D_j| \rangle = \frac{1}{N} \sum_{j=1}^{N} |D_j|. \qquad (6)$$

Thus, at each scale δE the coefficients $W_j(\delta E)$ give a normalized measure of the fluctuations at that scale, independent of the magnitude of the original spectrum. Finally, an entropy K is constructed to quantify the scale dependence of the fluctuations

$$K(\delta E) = -\frac{1}{N} \sum_{j=1}^{N} W_j(\delta E) \log W_j(\delta E). \qquad (7)$$

In the case of statistical fluctuations of $\sigma(E)$, the entropy K is constant. A change in the behavior of K is a signature for the appearance of a characteristic scale in the data. As more such scales are introduced at decreasing values of δE, the entropy should increase to a maximum. From the steplike increase in $K(\delta E)$ the characteristic scales of the data can be extracted.

The authors of Ref. [13] have shown that a suitable model for the steplike increase can be obtained from a Fermi-Dirac-like function

$$K(\delta E) = \sum_{i=1}^{m} \frac{k_i}{1 + \exp\left[\frac{\ln(\delta E) - d_i}{\Delta_i}\right]}, \qquad (8)$$

where there are m scales and k_i, d_i, and Δ_i are parameters obtained by a fit to the data. The characteristic energy scales $(\delta E)_i = s_i$ of structures in the data can be related to the parameter k_i by an empirical factor $K(s_i) = (0.92 \pm 0.01)k_i$ for each component i [18].

In principle, obtaining the scales is straightforward and the method has been applied [18] with some success on experimental data and model calculations (both, however, different from the ones analyzed in this article) of the ISGQR in ^{208}Pb. In practice, however, the method shows sensitivity to any peculiar features of the data, e.g., underlying background and the choice of the boundary conditions, and structures appear in the entropy index whose origin is not clear. A particular shortcoming of the method is that there is no possibility of reconstructing the spectrum on different scales to assess the importance or localization of a scale. In addition, the entropy as defined does not have the expected property of entropy; in particular it is not extensive. Thus, the entropy from two adjacent regions cannot be combined into a single entropy by addition. This again impacts on the localization of the scales.

It should be noted that the coefficients D_j that have been defined are in essence the coefficients of a wavelet analysis (discussed in Sec. VI below), in this case a continuous version of the Haar wavelet. Thus, the entropy index can also be calculated from the coefficients of a continuous wavelet transform using the Haar wavelet. Presumably, a similar entropy could be defined for other wavelet families, where the general characteristic of the Haar wavelet is maintained, i.e., for families that also yield a coarse-grained derivative of the spectrum. Although our use of the wavelet transform discussed in the next section has been motivated by this observation, we have found it more convenient to work with the wavelet coefficients directly.

B. Results

The entropy index as a function of the scale δE extracted from the present experimental and theoretical data sets is shown in Fig. 4. Energy scales at 100 keV, 420 keV, and 1.5 MeV are extracted by fitting the index with a sum of Fermi-Dirac functions. The solid line shows the fit according to Eq. (8) and the dashed lines the individual contributions for a certain value of i. Applying the method to an excitation energy range of 7.6 to 11.7 MeV in experimental (e, e') and (p, p') data on ^{208}Pb [5], intermediate scales were found at energies of 125 keV, 460 keV, and 1.1 MeV and confirmed by second-random phase approximation (SRPA) calculations [18]. Using these scales provides a reasonable description of the present experimental data as well. In the QPM calculations scales at 180 and 760 keV are suggested.

However, it is clear that there is additional structure in the analysis of the experimental data in the region of $\delta E = 200$–400 keV, as well as around 700 keV in both data sets, which does not easily fit into the scheme of the EIM because it would imply a *decreasing* entropy. It is our experience from the analysis of a variety of data that this type of structure can occur quite easily in the EIM analysis for no apparent reason.
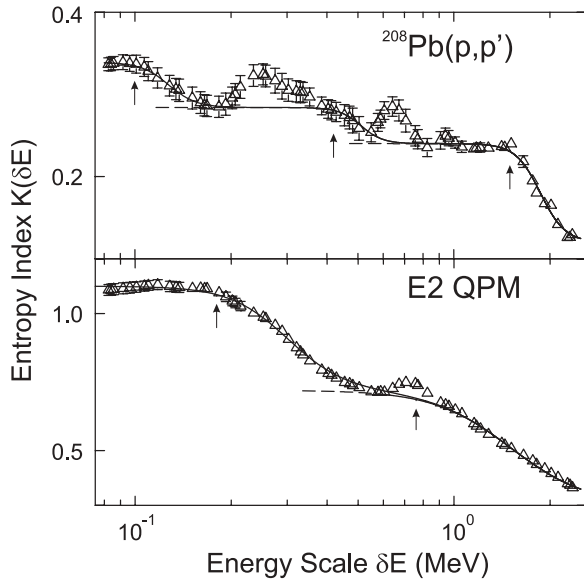
FIG. 4. Results of analysis by the entropy index method. The top and bottom panels show the analysis of the experimental and theoretical spectrum, respectively. The arrows indicate possible scales at 100 keV, 420 keV, and 1.5 MeV in the experimental data and at 180 and 760 keV in the QPM results, respectively, revealed by the fitting procedure discussed in the text. The dashed lines are the individual fits of Fermi-Dirac functions and the solid line the sum, Eq. (8).

This represents a limitation of the method which prevents an unambiguous determination of scales.

V. FOURIER TECHNIQUES

A. Method

The wavelet analysis discussed in the next section is often regarded as a generalization of the Fourier analysis. As an introduction to the wavelet methods, we discuss this classical technique. Here, we focus on the use of the Fourier power spectrum or some estimator thereof. By the Wiener-Khinchin theorem, the autocorrelation function and the power spectrum are Fourier transforms of one another. Thus, the two techniques are, in a sense, equivalent. However, for our purposes the form of the analyzed data is more satisfactory using the power spectrum. If $f(x)$ is a function of some quantity x and $\hat{f}(k)$ is the Fourier transform of f, the Fourier power spectrum is given by

$$P_f(k) = |\hat{f}(k)\hat{f}^*(k)|,\qquad(9)$$

up to some normalization of the spectrum.

Here, some remarks are in order. A spectrum can be regarded as a strength function [19,20]

$$S(E) = \sum s_i \delta(E - E_i),\qquad(10)$$

consisting of discrete peaks i with individual strengths s_i. Typically, physical effects and experimental resolution lead to a broadening of the peaks by convolution with a function such as a Gaussian. The power spectrum of this, i.e., the square of its Fourier transform, has a zero frequency component

determined by the total strength, with a rapid decay as a function of frequency determined by the overall envelope of the spectrum. This rapid decay will also be influenced by any windowing of the data. The bulk of the spectrum has a "noisy" character related to all possible differences $E_j - E_i$, giving rise to essentially random phases of the Fourier transform. The convolution with a resolution function leads to a slow modulation and cutoff of the power spectrum over a range characteristic of the width of the resolution function, the relatively narrow resolution function giving rise to a broad peak in the Fourier domain. Additional structure arises from correlations between the energy levels [19,20].

This picture is illuminating and some of these features are obvious in our data. However, the effect of multiple scales leads to additional complexity, making it unclear how to proceed with analysis. In addition, the strong localization present in our data questions the assumption of stationarity that underlies the technology of Fourier analysis.

B. Results

The Fourier power spectra of the two data sets are shown in Fig. 5. Note that they are plotted unconventionally against the energy rather than the reciprocal of energy (i.e., against $s = 2\pi/k$ rather than k) to enable a comparison with the wavelet analysis reported below. The analysis of the experimental spectrum is rich in structure but it is unclear how to interpret this. However, one may take some guidance from the fact that the experimental resolution produces a cutoff below $\simeq 50$ keV. Thus, structure below this energy must be statistical noise. Above this cutoff we can identify peaks at 70, 80, 130, and 200 keV (and perhaps 100 keV) potentially indicating significant scales in the data. The QPM results exhibit scales at 60 and 110 keV and eventually around 1 MeV, although
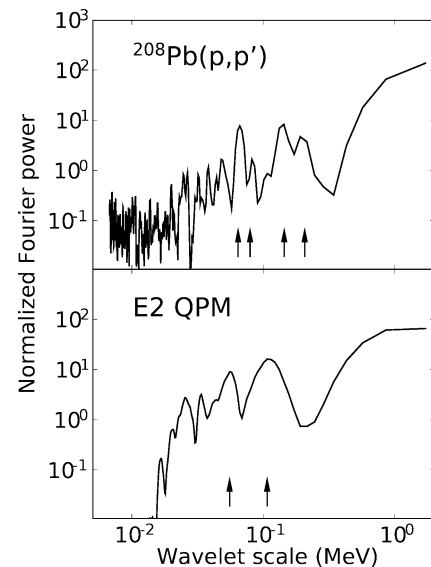

FIG. 5. Fourier power spectra, Eq. (9), of the data sets described in Sec. II normalized to the data variance. The arrows indicate possible scales at 70, 80, 130, and 200 keV in the experimental data (top) and at 60 and 110 keV in the QPM calculation (bottom).

for the latter the power spectrum does not show a pronounced maximum but becomes approximately constant toward larger scale values.

VI. WAVELET ANALYSIS

An increasingly popular method for the analysis of nonstationary time series is that of wavelet analysis, developed over the past two decades. In the language of signal processing, it is a method of analyzing signals by using a "wavelet" localized in both frequency and time domains [21,22]. A wavelet transform yields a set of coefficients that contain a representation of the data, which in the present case depends on the structure scale δE and the energy location E.

There are two fundamental types of such wavelet transform: the continuous (CWT) and the discrete (DWT). The discrete version is orthogonal and thus exactly invertible. However, the scales related are strictly ordered by factors of 2. Thus, the scale information lacks detail. The continuous transform, however, can have scales at arbitrary intervals but contains redundant information. Because the continuous wavelet basis is nonorthogonal and nonindependent, reconstruction of the data is overdetermined and thus more difficult and ambiguous. For the present purposes, however, the continuous transform offers greater flexibility. We compare both methods below, concentrating more on the CWT.

A. Continuous wavelet transform: Method

The transform depends on a wavelet function $\Psi(x, s)$ that is allowed to vary in both position x and scale s. In addition, it must satisfy certain admissibility conditions, basically that it has zero mean and is square integrable [21,22]. For the present application, the CWT is then defined by

$$C_i(\delta E) \equiv C(\delta E, E_x) = \frac{1}{\sqrt{\delta E}} \int \sigma(E) \Psi^* \left(\frac{E_x - E}{\delta E} \right) dE, \tag{11}$$

where position x can be identified with the excitation energy E_x in the spectrum and δE describes the energy scale. In practice, this integral is efficiently performed using the fast Fourier transform. As is usual, the data are binned into channels of constant energy width, referring to an energy bin at E_i by its index i. The integral thus becomes a sum over a finite grid of points. It is convenient to choose scales based on a fixed factor between adjacent scales

$$\delta E_j = \delta E_0 \, 2^{\frac{j}{n}}, \tag{12}$$

where δE_0 is the smallest scale and n divides each factor of two into subintervals. Typically, δE_0 is taken to be the spectrum energy bin and $n = 16$.

The set of coefficients $C_i(\delta E)$ obtained in such an analysis can be represented by a suitable plot, such as is illustrated in Fig. 6, where the Morlet wavelet [22]

$$\psi_{\text{Morlet}}(x) = \pi^{-1/4} e^{ikx} e^{-x^2/2} \tag{13}$$

has been used as a basis function. The parameter k weighs the resolution in scales versus the resolution in localization. To satisfy the admissibility conditions, $k \lesssim 5$ must be fulfilled. The examples discussed below use a value $k = 5$.
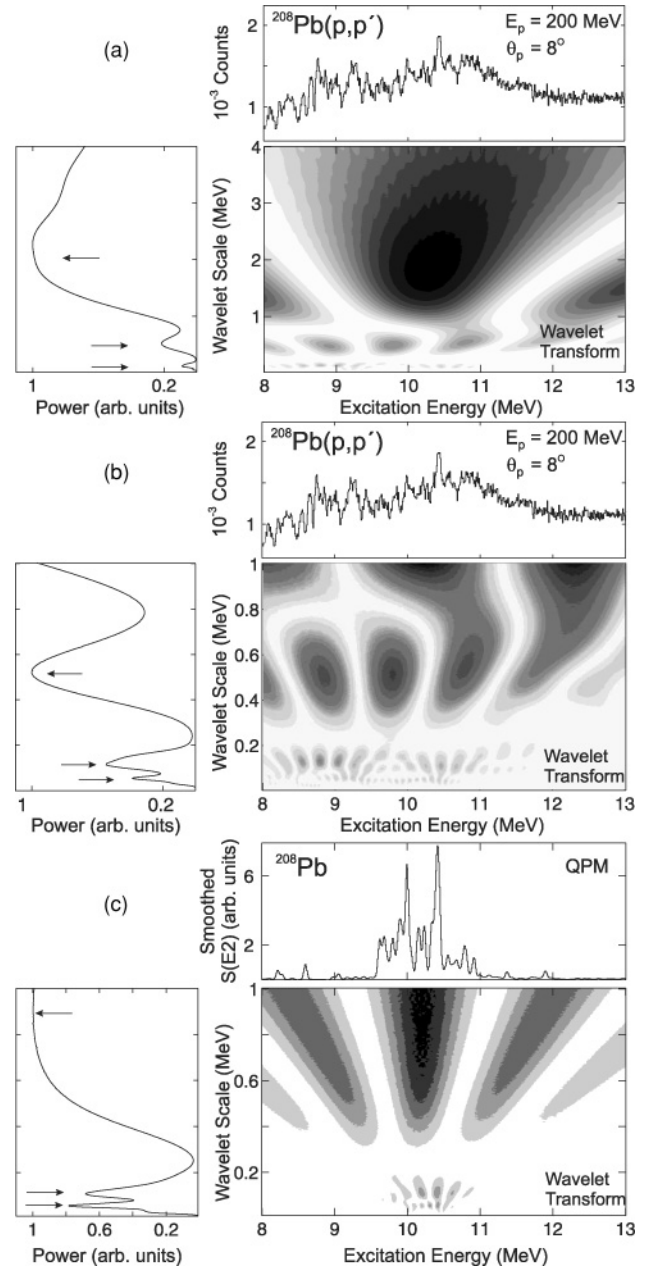

FIG. 6. Application of the CWT to the experimental and theoretical data sets. (a, top) Experimental spectrum over a range of excitation energy corresponding to the ISGQR. (Lower right) Density plot of the square of the CWT coefficients of the data using a complex Morlet wavelet. Lower left: total wavelet power as a function of scale obtained by projection onto the ordinate. (b) Same as (a) but for a restricted region of interest in scale (0–1 MeV). (c) Same as (b), but for the QPM strength function. The arrows indicate scales observed at 50 keV, 110 keV, 500 keV, 1.1 MeV, and 2.5 MeV in the experimental data and at 55 keV, 110 keV, 850 keV, and 1.4 MeV in the QPM calculation.

The wavelet mother function that is shifted and dilated in Eq. (11) defines a family of wavelets. Numerous basis functions are available, each having some intrinsic scale. A large overlap between the data and a wavelet of a particular value of δE and E_x leads to a large (positive or negative) value of the wavelet coefficient. Thus the CWT essentially determines the match between the data and the wavelet at some scale and position.

In Fig. 6, the square of the wavelet coefficients is plotted as a function of both energy and scale for a selected energy range $[E_1, E_2]$ of interest, for example, that of the ISGQR. The wavelet power spectrum is obtained by summing over the N energy bins in this range. We may define the wavelet power spectrum, which depends on the scale δE, by

$$P_w(\delta E) = \frac{1}{N} \sum_{i=i_1}^{i_2} |C_i(\delta E)C_i^*(\delta E)|. \quad (14)$$

Peaks in these power spectra can then be identified with important scales in the data.

B. Continuous wavelet analysis: Results

The results of a continuous wavelet transform of the experimental spectrum are presented in Fig. 6. In the top panel, Fig. 6(a), the spectrum is shown for the excitation region of the ISGQR in ^{208}Pb. The two-dimensional density plot below shows the squared wavelet coefficients as a function of excitation energy and scale. Dark regions correspond to large coefficients, whereas light regions correspond to regions with low wavelet power. It is clear that the fluctuations are localized in both energy and scale. This demonstrates an advantage of the wavelet method over other techniques like the entropy index method, the local scaling dimension, and the Fourier power spectrum. These supply only global information and no information about localization of structure that can lead to an optimization of the boundaries of the region of interest. In the present case, the plot can be restricted to the energy region $E_x = 8$–13 MeV. The wavelet analysis is shown again in Fig. 6(b) for scale values up to 1 MeV to demonstrate the presence of large coefficients at smaller scales as well. Finally,

the same analysis is applied to the QPM strength function, displayed in Fig. 6(c).

To achieve a more quantitative assessment of the characteristic scales, the sum of the squared wavelet coefficients in the region of interest is projected onto the scale axis. This gives rise to the wavelet power spectra shown in the left-hand panels of Fig. 6. From the peaks in this spectrum, intermediate characteristic scales of 110 keV, 500 keV, 1.1 MeV, and 2.5 MeV were extracted from the (p, p') data. An additional scale appears at about 50 keV; however, this is simply arising from the experimental resolution. In a similar analysis applied to the model spectrum based on the QPM, scales are observed at 55 keV (again, the trivial one), 110 keV, 850 keV, and 1.4 MeV.

As an illustration of the significance of structure in the wavelet power spectrum we compare in Fig. 7 the analysis for two energy regions in the experimental data. One region has considerable fine structure, and one at a higher energy has fluctuations which are expected to be of a statistical nature. The resulting wavelet power distributions normalized relative to each other clearly show that indeed one finds scales associated with the fine structure; in the other case power on all scales in the region of interest is small.

Most results we quote have been obtained from the structure of the wavelet power spectrum. This is closely related to the Fourier power spectrum as discussed below. However, the full utility of the wavelet analysis is represented by the plot of wavelet coefficients against excitation energy and scale. This allows an easy identification of regions of significant or little structure. It is also easy to identify any energy dependence of structure that is averaged out in the projection onto a power spectrum. Thus, the wavelet coefficients are invaluable in a full analysis.

Further verification of the nature of the fine structure is given by a reconstruction of the spectrum from the wavelet coefficients. This permits a restriction to significant scales and allows a comparison with the original spectrum. However, there is some ambiguity in this process owing to the redundancy in the nonorthogonal continuous wavelet coefficients. This seems to be mitigated to some extent by the use of scales in a logarithmic sequence. Given a set of coefficients, the original spectrum can be approximately
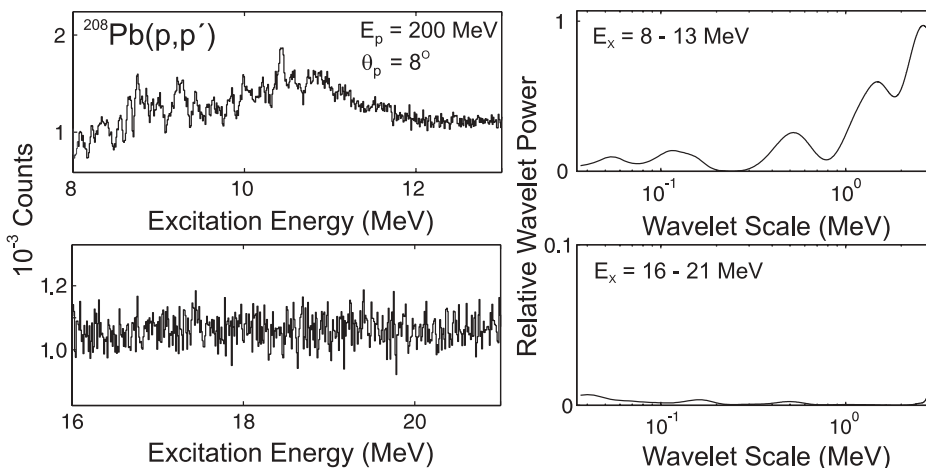

FIG. 7. Comparison of scales in different regions of the experimental data. (Top) Data in the region of the ISGQR (left) and the resulting wavelet power as a function of scale (right). (Bottom) Results for a region of higher excitation energy, where no fine structure is expected.

reconstructed as [22]

$$\sigma(E) = \frac{1}{C_\delta} \iint C(\delta E, E_x) \frac{1}{(\delta E)^{5/2}} \Psi$$
$$\times \left(\frac{E_x - E}{\delta E} \right) d(\delta E) \, dE_x, \qquad (15)$$

where C_δ is a normalization constant dependent on the wavelet family.

To demonstrate the significance of these scales we show the approximate reconstruction of the experimental spectrum in Fig. 8. The Morlet wavelet, Eq. (13), was used as the basis function for the initial decomposition. The top figure shows the original spectrum together with a reconstruction based on the largest scales, $\delta E = 0.8$–3 MeV; subsequent figures show the effect of adding in significant wavelet scales as indicated (cumulative from the top down). Note that most structures in the spectrum are accounted for by using the significant scales only. The final figure shows the result from a reconstruction using all the wavelet coefficients. It is clear that, despite the redundancy of the continuous wavelet basis, a good reconstruction can be achieved.

C. Discussion on various aspects of wavelet analysis

A number of questions concerning the wavelet analysis may arise, and we attempt to address some of these below.

1. How arbitrary are the scales?

The intrinsic scale of a particular wavelet basis function has a certain arbitrary character: it is chosen more for functional simplicity than any physical or mathematical characteristic of the wavelet. Thus, if any comparison between different wavelet families is made, a conversion factor between the scales of these two families must be introduced. This factor is a constant for a given wavelet family due to the linearity of the transform. The conversion is conveniently achieved by relating the scale of a particular wavelet family to the scale introduced by a Fourier transform [16]; in practice the two should agree on, say, the wavelength of a sinusoidal function. All scales can then be normalized to this "Fourier scale." A direct link between Fourier and intrinsic scale can be made for the case of the complex Morlet function, which should give identical scales. In turn, all other wavelet families can easily be normalized to the latter. The normalization is obtained from the main component of a Fourier analysis of the mother wavelet via the inverse Fourier transform. Because of the physical nature of the scales suggested for the decay of giant resonances in nuclei [1,2,6] we prefer to use a "wavelet scale," related to the Fourier scale by another constant factor, determined as described in Sec. II B.

2. Do different wavelet families give the same result?

The wavelet analysis is sometimes viewed as a tool that is useful for qualitative results but that has a certain quantitative ambiguity. It is thus important to show that different wavelet
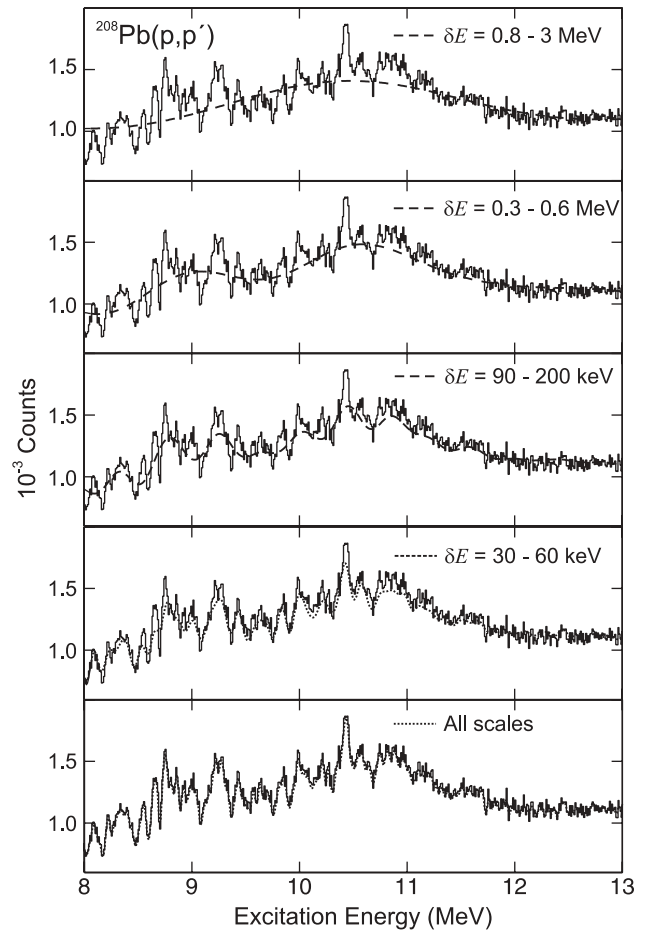

FIG. 8. Reconstruction of the spectrum using CWT. The top panel shows the original spectrum (histogram) together with the reconstruction based on scales between 0.8 and 3 MeV (dashed line). The three panels below show the effect of adding significant scales in the energy intervals indicated, to the reconstruction in the figure above; the bottom panel shows the spectrum reconstructed with all significant scales.

families give similar results. This is not obvious when viewing the plots of the coefficients but by comparing the wavelet power spectra, as in Fig. 9, it can be seen that the different families indeed do so. Of course, for this comparison all wavelet scales must be converted to the same Fourier scale as discussed above.

Figure 9 demonstrates that similar structures are obtained for all wavelet families; however, they differ in their ability to resolve details in the scales. For a particular experimental spectrum this depends (in addition to the type of data) on the response function of the detector. In the present case it is well approximated by a Gaussian, which makes the Morlet wavelet a preferred choice for our applications because it contains a Gaussian envelope superimposed on the sinusoidal structure. We also note that an application of the complex Morlet and a restriction to the real part gives only essentially identical results. Therefore, in practice we restrict the analysis to using the real part of the Morlet wavelet function.
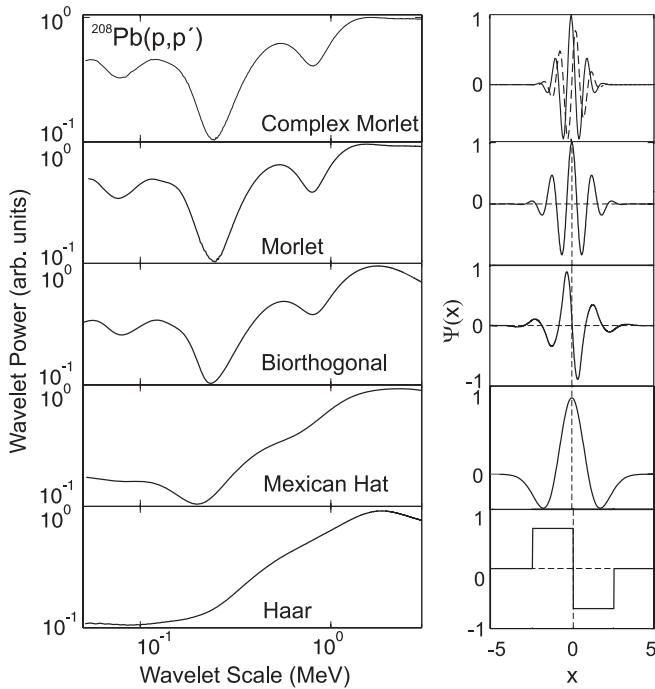
FIG. 9. Comparison of wavelet power spectra for the experimental data, as determined from different wavelet families. Note that the power spectra are plotted with a logarithmic scale. The left-hand panels show the wavelet power spectra and the right-hand panels the mother wavelet used in the corresponding continuous wavelet transform. For the complex Morlet wavelet, the solid and dashed lines indicate the real and imaginary part, respectively.

3. *How are scales chosen for the analysis?*

Scales naturally differ from one another by a factor rather than an increment. It is thus useful to choose scales that are equally spaced on a logarithmic axis. With the DWT discussed below these scales differ from one another by integer powers of 2. A convenient choice for the CWT is given by Eq. (12). In addition, the localization in scale of a structure is proportional to the scale, so the resolution in the power spectrum is uniform when plotted on a logarithmic scale axis.

4. *What data preconditioning should be applied?*

For Fourier analysis there has arisen a great deal of lore regarding the preconditioning needed to get the best results from the data. With wavelet analysis a great deal of this is not needed. For instance, windowing of the data is theoretically obscure for the wavelet transform and in any case would distort local structure in the data.

One problem that does require addressing is that of edge effects: the boundaries give rise to a cone of influence that extends to larger portions of the coefficients as the scale increases. Two methods can be used to treat this. First we note that the range of our interest in the present example is at excitation energies of 8 to 13 MeV. The CWT can be performed on the full spectrum, with a range of 0–22 MeV, and then the region of interest can be later isolated, with coefficients at low and high energies discarded. Alternatively,

the region of interest can be isolated before the transform and protected against end effects by padding both left and right sides; this can be done by padding with zeros, by padding with a functional form that tends rapidly to zero [23], or by continuing the spectrum at a constant value from the boundary of the region of interest to the edges of the original spectrum. This latter method tended to give the least edge effects in the coefficients [24] and was used to extract the scales given in Sec. VI B.

5. *How sensitive are the results to variations of the background?*

In contrast to the LSD and EIM approaches, the wavelet analysis shows little sensitivity to varying background conditions. Wavelet functions exhibit the feature of vanishing moments defined by

$$\int E^n \Psi(E)\, dE = 0 \quad \text{with} \quad n = 0, 1 \ldots m. \tag{16}$$

Therefore, any background in the spectrum, whether instrumental or due to physical processes, does not contribute to the wavelet coefficients if it can be approximated by a polynomial of order m.

6. *What measures of significance are there for peaks in the wavelet power spectrum?*

It can be shown that the average power per channel is given by the signal variance [16]. For a noise signal, a similar power would appear in each channel and the wavelet power spectrum normalized to the signal variance would have a mean value of 1. With a real signal, the extent to which the peak is greater than unity is a measure of the significance of the peak.

D. Discrete wavelet transform: Method

A choice of scales based on powers of 2 leads to the discrete wavelet transform [21,22]. It can be viewed as an iterative decomposition in the form of high-pass and low-pass filtering of the data yielding sequences of details (D_i) and approximations (A_i). At each level of decomposition $A_i + D_i = A_{i-1}$. At the first level of decomposition, $A_1 + D_1 = \sigma(E)$, where $\sigma(E)$ is the original spectrum. This decomposition method is illustrated in Fig. 10.

A key point is that the transform leads to an orthogonal decomposition of the spectrum from which exact reconstruction is possible. This makes direct comparison of the influence of characteristic scales possible. However, the resolution in scale is limited as scales are related to one another by integer powers of 2.

E. Discrete wavelet analysis: Results

The results of the decomposition of the experimental spectrum into its approximations and details A_i and D_i are illustrated in Fig. 11 using the experimental data set as example. Because the Morlet wavelet function does not
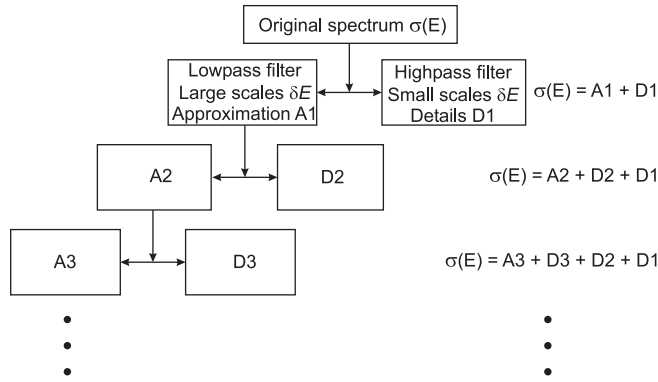
FIG. 10. Block diagram of the decomposition technique based on the discrete wavelet transform.
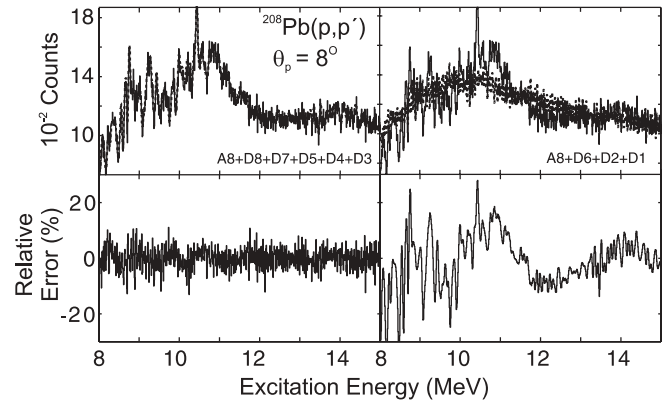

FIG. 12. (Top) Reconstruction of the experimental data set (histogram) from the coefficients of a DWT decomposition using selected subsets of the details D_i as indicated (dashed lines). (Bottom) Relative errors obtained by comparison with the exact spectrum.

allow for an orthogonal decomposition, the so-called BIOR3.9 wavelet [22] was used in this analysis. The plots represent the contribution of particular wavelet coefficients to the overall spectrum. The approximation coefficients illustrate how the background evolves as the index of the coefficient increases from 1 to 9. The D_i coefficients show the deviations from the approximation at a given scale. They provide a measure at which scales fluctuations in the spectrum are important. It is also clear that significant structure can be localized in energy. For example, the 96–192 keV scale has significant fluctuations in the region 8–12 MeV but little strength at higher energies.

A reconstruction of the experimental spectrum can be also be attempted using a limited set of the coefficients. If only "significant" scales are included in this reconstruction, an assessment of their significance can be made [25]. For instance,

Fig. 12 shows the reconstruction of the experimental spectrum by using the coefficients of $A_8 + D_8 + D_7 + D_5 + D_4 + D_3$. The fluctuations in the spectrum are reproduced remarkably well, as shown by the relative errors in the bottom left panel. However, reproduction with scales that would seem to be less significant ($A_8 + D_6 + D_2 + D_1$) leads to much larger errors, as shown in the bottom right-hand panel.

Thus, with the DWT analysis it is possible to isolate scale regions that carry significant information about the fluctuations in the spectrum and to test this significance directly by reconstruction. However, the basic scales are related by factors of 2, with the result that the power is not particularly well localized in scale. For instance, if a significant scale lies close
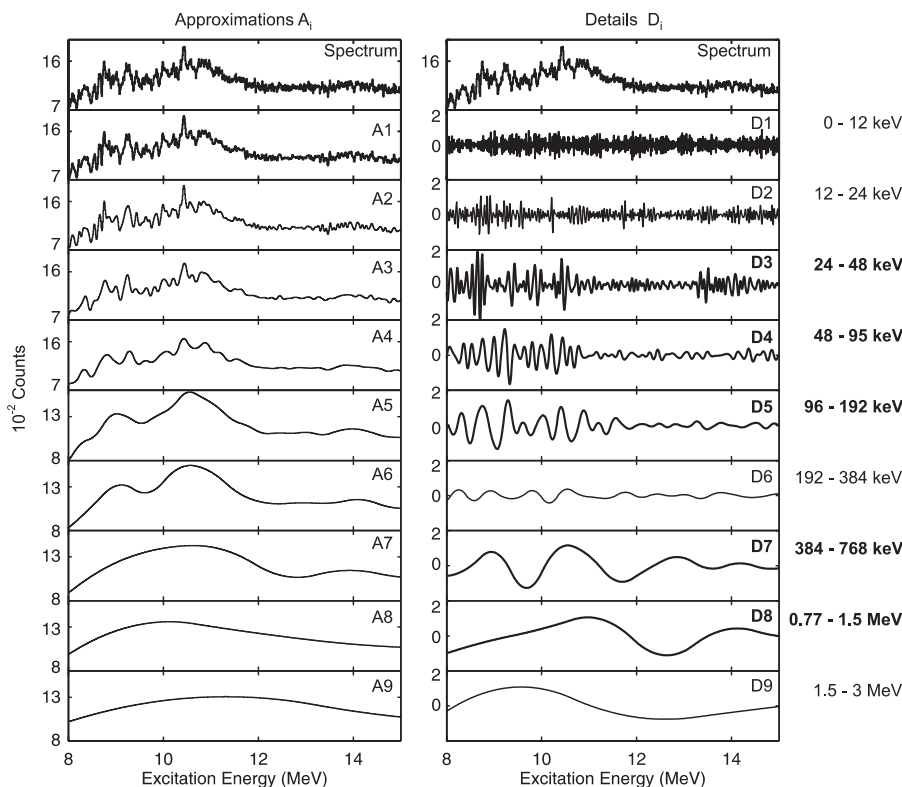

FIG. 11. Approximation (A_i) and detail (D_i) spectra obtained from the DWT coefficients for the experimental spectrum. The corresponding scale regions are given on the right-hand side and those marked in bold are considered important for the approximate reconstruction of the spectrum shown in Fig. 12.
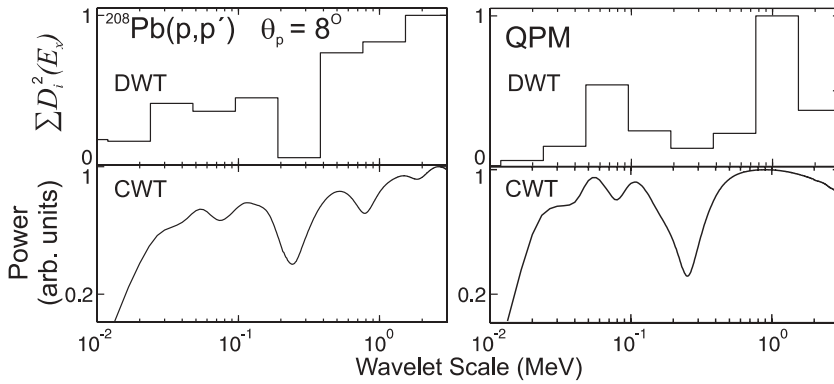
FIG. 13. Comparison of power spectra deduced from the experimental data with the DWT and the CWT.

to the boundary between two scale increments, the power will be distributed over both ranges.

In passing we note another important application of the DWT discussed in Ref. [10]. The property of vanishing moments [Eq. (16)] of wavelet functions allows to determine background with a smooth energy dependence in the giant-resonance region of the experimental spectrum based on the DWT decomposition. Combining this feature with a fluctuation analysis [15], level densities can then be extracted from the fine structure in a nearly model-independent way. This permits, e.g., experimental tests [26] of claims of a parity dependence of the level density in certain mass regions [27,28].

F. Comparison of CWT and DWT

The two forms of wavelet analysis are of course related. It is thus gratifying that there is a strong consistency between the CWT and DWT analyses. This consistency is demonstrated in Fig. 13, where we compare the CWT wavelet power spectrum and the sums of the squared detail coefficients from the DWT. A strong correlation of the two is observed. These results suggest that the CWT offers some advantages in that a clearer view of the strengths of the scales is achieved. For instance, the breadth of the peak in the region around 100 keV in the analysis of the experimental data hints at a doublet, whereas this is compressed into a single relative maximum by the DWT.

We have also shown in Fig. 12 that the discrete wavelets can be used for spectrum reconstruction to test the relevance of different scales. In this case the transform is orthogonal and the reconstruction can be exact; the limitation is in the coarseness of the scales. An approximate reconstruction is possible with the CWT as demonstrated in Fig. 8. However, the remaining deviations depend on the choice of the wavelet function and on the particular data sets.

G. Comparison of CWT and Fourier analysis

Finally, in Fig. 14 the wavelet power spectra from the CWT are compared with the Fourier power spectra; both are normalized to the data variance. There is good agreement between these two spectra: in fact, the wavelet and Fourier power spectra are related by

$$P_w(s)/s = \int P_f(k) \, |\hat{\psi}_0(sk)|^2 \, dk, \qquad (17)$$

where $\hat{\psi}_0(sk)$ is the Fourier transform of the wavelet mother function. We note that the square of the Fourier transform of a wavelet function is typically a bell-shaped function centered at s. Thus the wavelet power spectrum is a smoothed version of the Fourier power spectrum.

An interesting feature of the Fourier spectrum is its apparently greater detail. Although there is a suggestion of doublets of the peaks observed in the wavelet power spectrum in the regions around 100 and 200 keV, it is not clear whether this is a real effect in the Fourier spectrum or arises because of the constraints of matching a nonstationary spectrum with Fourier components. It is notable in the reconstruction of this scale as shown in Figs. 8 and 11 that the amplitude of the coefficients varies quite strongly over the energy region. This effect can be obtained only with a Fourier analysis by addition of several components.

It is also worth noting that reconstruction of this scale region from a single wavelet component gives a similar picture; if this reconstruction is Fourier analyzed, two frequencies are found. Thus, a single wavelet scale has to be represented by two Fourier analysis scales. The Fourier analysis has the possibility of giving greater resolution, whereas the wavelet
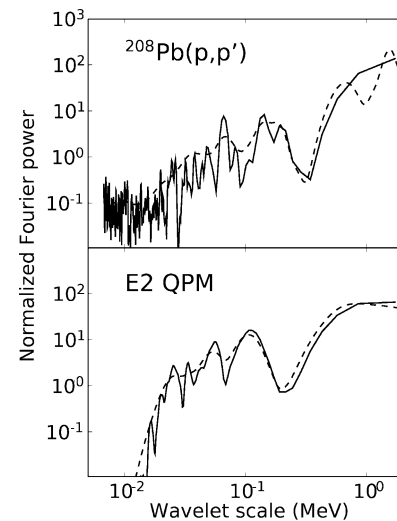

FIG. 14. Comparison of Fourier power spectra (solid lines) and CWT power spectra (dashed lines) for the two data sets as a function of the wavelet scale. All spectra are normalized to the data variance.

analysis clusters closely spaced scales into a single group. Both of these techniques offer unique advantages. The CWT shows the localization of structure for a given scale; the Fourier transform will give clearer results for periodic or regularly spaced features.

VII. CONCLUDING REMARKS

In this article we described various methods for obtaining information on the scales of fine structure in nuclear spectra. As a typical example, used to demonstrate the various techniques, the fine structure of the ISGQR in ^{208}Pb has been investigated using an experimental data set and a theoretical calculation based on the QPM. The local scaling dimension method, the entropy index method, and the continuous and discrete wavelet transform have been applied to the analysis of the experimental data and the model strength function. In addition the results of a Fourier analysis have been explored.

We have shown that wavelet analysis, both continuous and discrete, is a particular promising tool to obtain information

on the scales of the fine structure. The analysis reveals clear signatures of the various important scales that occur in the demonstration spectra. Indeed, we have found that this signature extends to other nuclei and other types of giant resonances as well. However, the nature of this information is not easy to interpret in isolation and requires comparison with theoretical results (see, e.g., Refs. [6,10]). A summary of our findings on the fine structure of the ISGQR observed in nuclei over a wide mass range and its implications for an understanding of the physical nature of the scales is subject of a forthcoming article.

[1] M. N. Harakeh and A. van der Woude, *Giant Resonances: Fundamental High-Frequency Modes of Nuclear Excitation* (Oxford University, Oxford, 2001).

[2] P. F. Bortignon, A. Bracco, and R. A. Broglia, *Giant Resonances: Nuclear Structure at Finite Temperature* (Harwood Academic, Amsterdam, 1998).

[3] A. Schwierczinski, R. Frey, A. Richter, E. Spamer, H. Theissen, O. Titze, T. Walcher, S. Krewald, and R. Rosenfelder, Phys. Rev. Lett. **35**, 1244 (1975).

[4] G. Kühner, D. Meuer, S. Müller, A. Richter, E. Spamer, O. Titze, and W. Knüpfer, Phys. Lett. **B104**, 189 (1981).

[5] S. Kamerdzhiev, J. Lisantti, P. von Neumann-Cosel, A. Richter, G. Tertychny, and J. Wambach, Phys. Rev. C **55**, 2101 (1997).

[6] A. Shevchenko, J. Carter, R. W. Fearick, S. V. Förtsch, H. Fujita, Y. Fujita, Y. Kalmykov, D. Lacroix, J. J. Lawrie, P. von Neumann-Cosel, R. Neveling, V. Yu. Ponomarev, A. Richter, E. Sideras-Haddad, F. D. Smit, and J. Wambach, Phys. Rev. Lett. **93**, 122501 (2004).

[7] S. Strauch, P. von Neumann-Cosel, C. Rangacharyulu, A. Richter, G. Schrieder, K. Schweda, and J. Wambach, Phys. Rev. Lett. **85**, 2913 (2000).

[8] A. Tamii, T. Adachi, J. Carter, M. Dozono, H. Fujita, Y. Fujita, K. Hatanaka, H. Hashimoto, T. Kaneda, M. Itoh, T. Kawabata, H. Matsubara, K. Nakanishi, P. von Neumann-Cosel, H. Okamura, A. Perez, I. Poltoratska, V. Yu. Ponomarev, L. Popescu, A. Richter, B. Rubio, H. Sakaguchi, Y. Sakemi, Y. Sasamoto, Y. Shimbara, Y. Shimizu, F. D. Smit, Y. Tameshige, M. Yosoi, J. Zenihiro, and K. Zimmer, Nucl. Phys. **A788**, 53c (2007).

[9] P. von Neumann-Cosel, F. Neumeyer, S. Nishizaki, V. Yu. Ponomarev, C. Rangacharyulu, B. Reitz, A. Richter, G. Schrieder, D. I. Sober, T. Waindzoch, and J. Wambach, Phys. Rev. Lett. **82**, 1105 (1999).

[10] Y. Kalmykov, T. Adachi, G. P. A. Berg, H. Fujita, K. Fujita, Y. Fujita, K. Hatanaka, J. Kamiya, K. Nakanishi, P. von Neumann-Cosel, V. Yu. Ponomarev, A. Richter, N. Sakamoto, Y. Sakemi, A. Shevchenko, Y. Shimbara, Y. Shimizu, F. D. Smit,

T. Wakasa, J. Wambach, and M. Yosoi, Phys. Rev. Lett. **96**, 012502 (2006).

[11] J. Winchenbach, K. Pingel, G. Holzwarth, G. Kühner, and A. Richter, Nucl. Phys. **A410**, 237 (1983).

[12] H. Aiba and M. Matsuo, Phys. Rev. C **60**, 034307 (1999).

[13] D. Lacroix and P. Chomaz, Phys. Rev. C **60**, 064307 (1999).

[14] V. G. Soloviev, *Theory of Atomic Nuclei: Quasiparticles and Phonons* (Institute of Physics, Bristol, 1992).

[15] P. G. Hansen, B. Jonson, and A. Richter, Nucl. Phys. **A518**, 13 (1990).

[16] C. Torrence and G. P. Compo, Bull. Am. Meteorol. Soc. **79**, 61 (1998).

[17] H. Aiba, M. Matsuo, S. Nishizaki, and T. Suzuki, Phys. Rev. C **68**, 054316 (2003).

[18] D. Lacroix, A. Mai, P. von Neumann-Cosel, A. Richter, and J. Wambach, Phys. Lett. **B479**, 15 (2000).

[19] L. Leviandier, M. Lombardi, R. Jost, and J. P. Pique, Phys. Rev. Lett. **56**, 2449 (1986).

[20] Y. Alhassid and N. Whelan, Phys. Rev. Lett. **70**, 572 (1993).

[21] I. Daubechies, *Ten Lectures on Wavelets*, SIAM, Vol. **61** (1992).

[22] S. Mallat, *A Wavelet Tour of Signal Processing* (Academic Press, San Diego, 1998).

[23] S. D. Meyers, B. G. Kelly, and J. J. O'Brien, Mon. Weather Rev. **121**, 2858 (1993).

[24] The CWT analysis in Ref. [6] was applied on the full spectrum, which leads to slightly different values for the scales compared to the ones given here.

[25] A. Richter, Prog. Part. Nucl. Phys. **55**, 387 (2005).

[26] Y. Kalmykov, C. Özen, K. Langanke, G. Martínez-Pinedo, P. von Neumann-Cosel, and A. Richter, Phys. Rev. Lett. **99**, 202502 (2007).

[27] Y. Alhassid, G. F. Bertsch, S. Liu, and H. Nakada, Phys. Rev. Lett. **84**, 4313 (2000).

[28] D. Mocelj, T. Rauscher, G. Martínez-Pinedo, K. Langanke, L. Pacearescu, A. Faessler, F.-K. Thielemann, and Y. Alhassid, Phys. Rev. C **75**, 045805 (2007).